Modelling of a Switchable Permanent Magnet Magnetic Flux Actuator

Imants Dirba, Janis Kleperis
Institute of Solid State Physics of University of Latvia, Kengaraga Street 8, Riga, Latvia
*Corresponding author: imants.dirba@gmail.com

Abstract: A simple magnetic circuit consisting of ferromagnetic core material, air gap, permanent magnets and current coils can be used to form magnetic actuators, motors etc. devices. In this work the current coils are not used to generate working magnetic field, but just to switch magnetic flux created by permanent magnets in necessary direction. Analytical and numerical (Finite Element Model, COMSOL) models are set up and solved; an experimental model of switchable magnetic flux linear actuator is constructed and tested. Obtained experimental results are compared with outputs from analytical and numerical models. Conclusions are made and further research steps are outlined.

Keywords: Electromagnetism, numerical modelling, switchable magnetic flux.

1. Introduction

The modelling of electrical machines is particularly important for studying their behaviour as well as in optimization tasks. Its methods can be categorized into the analytical modelling and the numerical modelling [1]. The analytical modelling has the advantage of rapidity, while its accuracy is not sufficient for optimization in a design process. At the same time, the numerical modelling is highly precise method but is time-consuming; nevertheless it is widely applied (see, e.g. [2,3]). Calculation in the applications needs accuracy, whereas the time of simulation is of less importance. The numerical method is based on the discrimination of a calculation domain to finite elements and solution of Maxwell's equations for these elements [4].

This paper presents a theoretical development and analysis of the results of experiments and 2D COMSOL simulation of the working principle of a PPMT linear actuator as well as the results obtained by calculation of the air-gap magnetic flux density and magnetic forces.

2. Model description

The parallel path magnetic technology (PPMT) uses two or more permanent magnets placed in parallel [5,6]. The basic magnetic circuit consists of a flux steering coil on each flux path as shown in Fig. 1. In the case there is no current in the coils, the magnetic circuit acts as if these coils are absent.

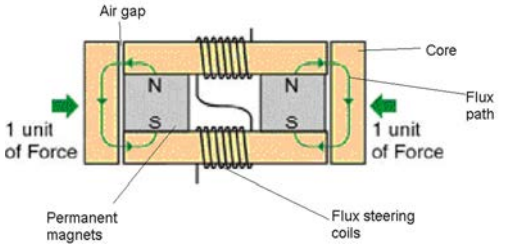

Figure 1. Basic PPMT actuator (flux steering coils off) [6].

However, if current flows in the flux steering coils to produce a magnetic polarity as shown in Fig. 2, the magnetic flux produced by the coils couples with the permanent magnet's flux, and the result is four units of force (instead of two in Fig. 1 due to the squared force law of the combined permanent magnet flux) at one pole of the device. A momentary coil pulse of the opposite polarity will switch the actuator in the opposite direction (Fig. 2).

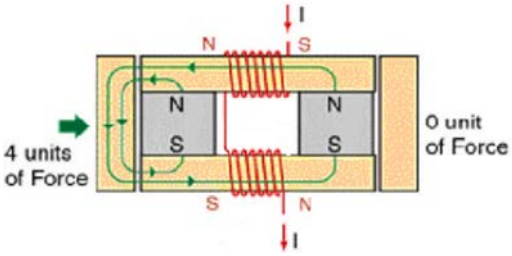

Figure 2. Basic PPMT actuator steering coils for switching the whole magnetic flux to one actuator pole [6].

In the actuation of a PPMT device the steering coil only needs to have sufficient current to equalize the flux of one permanent magnet. Thus in such a device a given amount of magnetic flux can be controlled with only half the field coil power required by conventional devices.

3. Simplified theoretical analysis of the PPMT device.

3.1. Simplified analysis of a PPMT device in the case of no current in the coils

The boundary condition of the magnetic flux density component normal to the

boundary between two environments (a and b in Fig. 3) with different permeability is:

$$B_{na} = B_{nb} \qquad (1)$$

The magnetic field in the air gap is approximately the same as in the conductor (since it is not dissipated). The line integral in Circulation Theorem of the magnetic field can be decomposed into the magnetic field for each field conductor (Fig. 3) [7]:

$$\oint_l \frac{\vec{B}d\vec{l}}{\mu} = \int_{l_m} \frac{\vec{B}d\vec{l}}{\mu_m} + \int_{l_2} \frac{\vec{B}d\vec{l}}{\mu_{Fe}} + \int_{l_g} \frac{\vec{B}d\vec{l}}{\mu_g} + \\ + \int_{l_1} \frac{\vec{B}d\vec{l}}{\mu_{Fe}} + \int_{l_g} \frac{\vec{B}d\vec{l}}{\mu_g} + \int_{l_2} \frac{\vec{B}d\vec{l}}{\mu_{Fe}} = \mu_0 nI \qquad (2)$$

where:

$B-$ is the magnetic field induction vector;

$l-$ is the contour path length;

$\mu-$ is the permeability of the material;

μ_0- is the magnetic constant (vacuum permeability);

$I-$ is the current in the loop;

$n-$ is the number of windings in the loop.

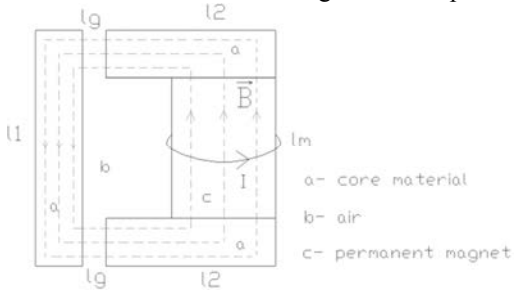

Figure 3. Schematic of parallel path core for the case with flux steering coils off (Fig. 1).

From Eq. (2) according to Fig. 3 the following relationship is obtained:

$$\frac{\vec{B}}{\mu_m} l_m + \frac{\vec{B}}{\mu_{Fe}} l_2 + \frac{\vec{B}}{\mu_g} l_g + \frac{\vec{B}}{\mu_{Fe}} l_1 + \\ + \frac{\vec{B}}{\mu_g} l_g + \frac{\vec{B}}{\mu_{Fe}} l_2 = \mu_0 nI \qquad (3)$$

In turn, from Eq. (3) the following equation for the air gap magnetic flux density is derived:

$$\Rightarrow \vec{B} = \frac{\mu_0 nI}{\frac{l_m}{\mu_m} + \frac{l_2}{\mu_{Fe}} + \frac{l_g}{\mu_g} + \frac{l_1}{\mu_{Fe}} + \frac{l_g}{\mu_g} + \frac{l_2}{\mu_{Fe}}} \qquad (4)$$

For identifying the term nI in Eq. (4), the permanent magnet is considered as material consisting of internal micro-currents [7], therefore the current loops inside the material are opposite and compensate each other. Thus we can only deal with the current loop lying on the surface of material. The Biot-Savart law relates magnetic fields to the currents which are their sources (Fig. 4) [8]. Therefore for the magnetic field induction in the centre of permanent magnet (if it is described with a current loop having radius vector r_o lying on the surface) we have:

$$B = \frac{\mu_0 I}{2r_0} \qquad (5)$$

Knowing the residual flux density, magnetic permeability, magnetic flux and sizes of the permanent magnet, the current in the current loop lying on the surface can be calculated as

$$I = \frac{B \cdot 2 \cdot r_0}{\mu_0 \mu} = \frac{1{,}2 \cdot 2 \cdot 0{,}006}{1{,}05 \cdot 4\pi \cdot 10^{-7}} = 10913\,A \qquad (6)$$

Therefore, the air-gap magnetic flux density can be derived from Eq. (4):

$$\Rightarrow \vec{B} = \frac{\mu_0 nI}{\frac{l_m}{\mu_m} + \frac{l_2}{\mu_{Fe}} + \frac{l_g}{\mu_g} + \frac{l_1}{\mu_{Fe}} + \frac{l_g}{\mu_g} + \frac{l_2}{\mu_{Fe}}} = \\ = \frac{4\pi \cdot 10^{-7} \cdot 10913}{0{,}03} \approx 0{,}45T \qquad (7)$$

where:

$\vec{n}-$ is the normal vector;

$\vec{r}_0-$ is the radius vector;

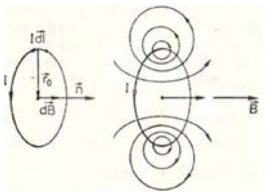

Figure 4. Biot – Savart law ([8]).

The force is calculated from Maxwell's stress tensor:

$$T_{ik} = \varepsilon_0 E_i E_k + \frac{1}{\mu_0} B_i B_k - \\ - \frac{\delta_{ik}}{2}\left(\varepsilon_0 \vec{E}^2 + \frac{1}{\mu_0}\vec{B}^2\right), [N/m^2] \qquad (8)$$

As forces are produced only by magnetic field, Eq. (8) reduces to:

$$T_{ik} = \frac{1}{\mu_0} B_i B_k - \frac{\delta_{ik}}{2}\frac{1}{\mu_0}\vec{B}^2, [N/m^2] \qquad (9)$$

From Fig. 5. it is seen that only the xx-component of Maxwell's stress tensor is left:

$$T_{xx} = \frac{1}{\mu_0} B_x B_x - \frac{1}{2}\frac{1}{\mu_0}\vec{B}^2 = \\ = \frac{1}{2}\frac{1}{\mu_0} B^2, [N/m^2] \qquad (10)$$

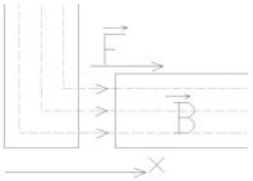

Figure 5. Geometry of the calculated force.

The width and height of the rectangular core cross-section is 25 mm, therefore the force for both core sides will be:

$$\vec{F} = \oint_{\sigma} T_{ik} d\vec{S} = T_{xx} \Delta S = \frac{B^2}{2\mu_0} S =$$

$$= \frac{0{,}45^2}{2\mu_0} \cdot 0{,}025 \cdot 0{,}025 \cdot 2 = 100N \quad (11)$$

3.2. Simplified analysis of PPMT device in the case with current in the coils

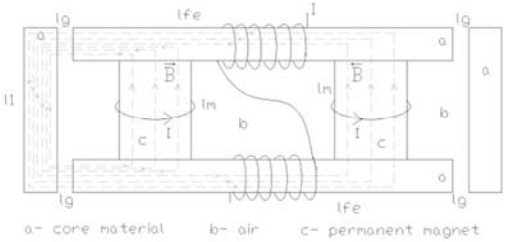

Figure 6. Schematic of the parallel path core for the case of steering coils engaged.

If we suppose that the core is not saturated, from the superposition principle the magnetic field induction in the air gap is found via summation of the value calculated by Eq. (7) and the values of magnetic field induction produced by the second magnet and by the current coils. Thus for the case shown in Fig.6 we will have:

$$\vec{B}_{\Sigma} = 0{,}45T + \frac{\mu_0 \Sigma nI}{\frac{l_m}{\mu_m} + \frac{l_{fe}}{\mu_{Fe}} + \frac{l_g}{\mu_g} + \frac{l_1}{\mu_{Fe}} + \frac{l_g}{\mu_g} + \frac{l_{fe}}{\mu_{Fe}}} = 0{,}90T \quad (12)$$

and, therefore, the force is

$$\vec{F} = \frac{B^2}{2\mu_0} S = \frac{0{,}90^2}{2\mu_0} \cdot 0{,}00125 = 402N \quad (13)$$

4. Numerical modeling of the PPMT device

2 dimensional Magnetic Fields (mf) problem has been set up in COMSOL Multiphysics version 4.2. System consists of ferromagnetic core material (a), air (b), permanent magnets (c) and current coils (d) as it is shown in Fig. 7. NdFeB permanent magnets are prescribed with using Amperes Law – given magnetization M in y axis direction. Current in the flux steering coils is given by External Current Density J_e in z axis direction.

In our case a 2D magnetic fields problem is considered, i.e. the magnetic field lines, vectors, air gap flux density, and force are plotted in a xy-plane. The core of the magnetic machine under consideration is made from four rectangle pieces of steel and permanent magnets (a and c, respectively, in Fig. 7). Current coils d are wound around two parallel core elements.

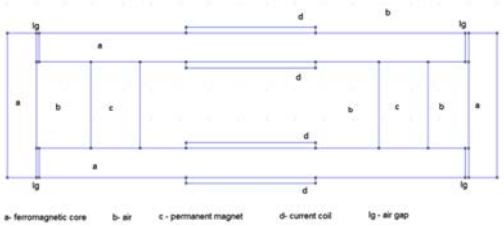

Figure 7. Geometry of the simulated magnetic system.

4.1. Numerical modelling of a PPMT device in the case without current in the coils

The output of numerical calculations for the geometry shown in Fig. 7 is displayed in Fig. 8, with magnetic field vectors in the system formed by permanent magnets depicted for the no-current case.

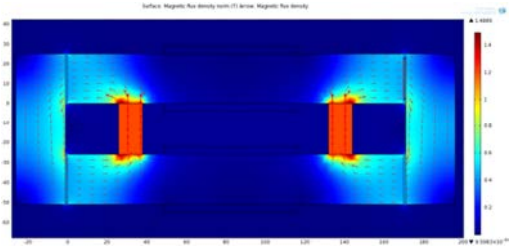

Figure 8. Simulation for PPTM in the no-current case: resultant magnetic field density, field lines and vectors.

The magnetic field density in the air-gap is shown in Fig. 9. As is seen, the magnetic field is not dissipated, so in the air-gap it is approximately the same as in the conductor.

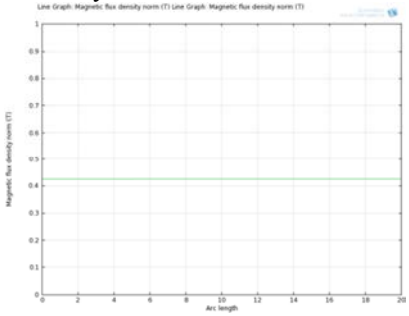

Figure 9. Magnetic flux density in the air-gap of the simulated magnetic system.

The core-side magnetic attraction force was calculated by COMSOL using Maxwell's stress tensor, and the resultant value of 91 N obtained.

4.2. Numerical modelling of a PPMT device in the case with current in the coils

Figure 10 shows the magnetic field lines and vectors for the system formed by permanent magnets in the case with steering coils (the output of numerical calculations for the geometry depicted in Fig. 2 is presented above).

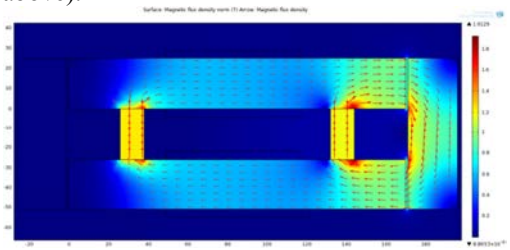

Figure 10. Magnetic field density, field lines, and vectors in the case of current in the coils.

The magnetic flux produced by the current coils couples with the permanent magnet's flux and the result is a doubled magnetic flux density. The ferromagnetic core is almost saturated, therefore it is impossible to apply stronger (N52) NdFeB magnets. The core-side magnetic attraction force was again calculated using Maxwell's stress tensor, and the value of 361 N obtained.

5. Experimental setup, comparison of the results

The experimental setup was made in compliance with the geometry shown in Fig. 8. A Zwick/Roell BDO-FB005TN machine for testing materials (Fig. 11) with the maximum tension load of 5 kN was used to experimentally obtain the core-side magnetic attraction force. A PPTM device was mounted in the testing machine and the required critical force values were identified in a stretching process. The experimentally determined core-side magnetic attraction forces, together with analytical and numerical calculation results, are presented in Table 1. As is seen from Table 1, the obtained analytical, numerical and experimental results are comparable, therefore it could be inferred that the theoretical model and simulation methods proposed in this paper are applicable. The smaller value of force (81N) in the experimental results is due to spacers – as the force value decreases almost four times compared with the case of Fig. 2, the linear size of these spacers increases; therefore, the air-gap flux density decreases, which leads to a reduced value of force.

Figure 11. Experimental setup: a Zwick/Roell BDO-FB005TN testing machine with a test sample.

Table 1: Comparison of the simulated and experimentally obtained results.

	Core-side attraction force, N	
Model	Case Fig. 2	Case Fig. 3
Analytical	100	402
Numerical	91	361
Experimental	81	305

The second experimental value is smaller than the numerical credible because of saturation effects in the core material (not taken into account in our simplified analytical model) and also the fringing effect of magnetic flux in the air-gap.

6. Conclusions

A two-dimensional finite element model has been used for accurate analysis of the working principle of a switchable PPMT actuator. The air-gap flux density and magnetic force values were calculated using the developed model, and it is shown that the simulation results are in a good agreement with the theoretically calculated (variation in the air-gap magnetic flux density values is only ~ 4.4%) and experimentally measured values.

If current flows in the flux steering coils producing the magnetic polarity, the produced magnetic flux couples with the permanent

magnet's flux, with the result being almost four units of force (instead of two due to the squared force law of the combined permanent magnet flux) at one pole of the device. In the actuation of the PPMT device a steering coil only needs to have sufficient current to equalize the flux of one permanent magnet. Thus, in the PPMT devices a given amount of magnetic flux can be controlled with only half power in the coil comparing to conventional electric machines.

7. Further research

In this paper we illustrated the basic working principle of the PPMT ideology. Further research on the PPMT motor will be done with the first prototype (Figs. 12.-13.) built according to the circuit sketched in 6].

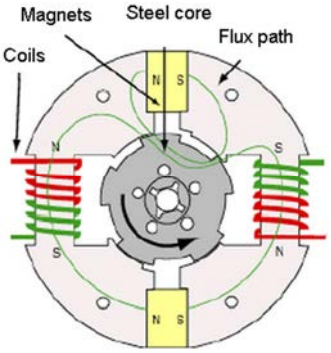

Figure 12. Switchable PPMT motor – basic circuit arrangement [6].

Figure 13. Switchable PPMT motor (the prototype).

8. References

1. Krishnan, R., (2001) *Electric Motor Drives: Modelling, Analysis, and Control.* Prentice Hall, 626.

2. Hameyer, K. (1999). Numerical Modelling and Design of Electrical Machines and Devices. *Book Series: Advances in Electrical and Electronic Engineering,* (1).

3. Vese, I.-C., Marignetti, F., & Radulescu. M.M. (2010). *IEEE Transactions on Industrial Electronics, 57,* 320 – 326.

4. Dolinar, D., De Weerdt, R., Belmans, R., & Freeman, E.M. (1997). *IEEE Transactions on Energy Conversion, 12,* 133-142.

5. Flynn, C.J. (1995). US Patent No 5455474.

6. C.J. Flynn, C.J., Talsoe, N.B., & Childress, J.J. (2006). Space Tech.& Applic.: 3rd Symp.New Frontiers & Future Concepts. *AIP Conf. Proceedings*, *813,* 1205-1212.

7. Feynman, R.P. (1971). *The Feynman Lectures on Physics,* vol. II, Addison – Wesley, 592.

8. Platacis, J. (1974). *Electricity: Lectures for Students.* Riga: Zvaigzne, 503 p.

9. Acknowledgements

The authors acknowledge Gatis Arents for technical assistance. We thank the Latvian National Research Program in Energetics and one from us (ID) thanks ESF (European Social Fund) for financial support in researches.